arXiv:astro-ph/9701092v1 15 Jan 1997

Electron Acceleration and the Production of Nonthermal Electron Distributions in Accretion Disk Coronae

Hui Li[1] and James A. Miller[2]

Received _____; accepted _____

[1]NIS-2, MS D436, Los Alamos National Laboratory, Los Alamos, NM 87545; hli@lanl.gov

[2]Department of Physics, The University of Alabama in Huntsville, Huntsville, AL 35899; miller@mpingo.uah.edu

ABSTRACT

We consider electron acceleration by obliquely propagating fast mode waves in magnetically dominated accretion disk coronae. For low coronal plasma densities, acceleration can exceed Coulomb drag at lower energies and energize electrons out of the thermal background, resulting in a nonthermal tail. The extent of this tail is determined by the balance between acceleration and radiative cooling via inverse Compton scattering and synchrotron emission, and usually goes out to tens of MeV. This will have direct applications for explaining the gamma-rays from several galactic black hole candidates, such as Cyg X-1 and GRO J0422, which show 0.5–5 MeV emissions in excess over what most thermal models predict. Detailed time evolutions of the particle distributions and wave spectra are also presented.

Subject headings: acceleration of particles — accretion, accretion disks — gamma rays: theory — waves

1. Introduction

Thermal Comptonization models have had much success in explaining the hard X-ray spectra from galactic black hole candidates (GBHCs) with the plasma temperature $\sim$ 50-100 keV and Thomson depths of a few (e.g., Shapiro, Lightman, & Eardly 1976; Sunyaev & Titarchuk 1980; Harmon et al. 1994; Liang 1993). However, the most sensitive observations of GBHCs to date in the 0.5–5 MeV range by *Compton* Gamma-Ray Observatory have clearly revealed that persistent gamma rays ($>$ 1 MeV) are being produced in some GBHCs, notably Cyg X-1 (McConnell et al. 1996; Phlips et al. 1996; Ling et al. 1996) and GRO J0422 (van Dijk et al. 1995). These gamma-ray emissions are very difficult to accommodate by the pure thermal models (e.g., Sunyaev & Titarchuk 1980; Titarchuk 1994), strongly suggesting the need for modification (Skibo & Dermer 1995) or to incorporate some nonthermal processes.

Recently, Li, Kusunose, & Liang (1996) have proposed a gyroresonant stochastic electron acceleration model to account for the MeV emissions from GBHCs (see also Dermer, Miller, & Li 1996). In that model, they showed that high frequency whistlers can accelerate electrons directly from the thermal background, after which Alfvén waves would continue the acceleration to higher energies. The result is an electron distribution with a hard non-Maxwellian tail. Compton scatterings from both thermal and nonthermal electrons produce a broad band X- to gamma-ray spectrum, in agreement with that observed from both Cyg X-1 and GRO J0422. One uncertainty associated with that model is the generation of whistlers, which can arise from either a cascade of wave energy from lower frequencies or a microinstability (see e.g., Gary 1993). While the nature of wave cascading is fairly well known in the MHD regime (e.g., Verma 1994; Roberts & Wiltberger 1995), it has not been investigated at higher frequencies. Producing waves that can gyroresonate with an electron of a given energy through a resonant microinstability

requires (among other things) an anisotropic electron distribution containing electrons of that energy. Nonresonant instabilities may also produce the needed waves, but still require specific anisotropic distributions.

In this *Letter*, we consider electron acceleration by MHD fast mode waves that likely exist in accretion disk coronae. These low-frequency waves can accelerate electrons from thermal to relativistic energies. Coupled time-dependent diffusion equations for the electron distribution and the wave spectral density are solved numerically (Miller, LaRosa, & Moore 1996, hereafter MLM). Nonthermal electron distributions are clearly obtained under a range of parameters in the accretion disk environment, which will have a direct bearing on the future modeling of the hard X-ray and gamma-ray emissions from GBHCs.

2. THE MODEL

2.1. Basic Model Assumptions and Parameters

The hydrogen plasma flowing around a black hole with mass M is assumed to form an accretion disk (e.g., Shakura & Sunyaev 1973), from which most of the soft photons (a few keV) originate. In the inner part of the disk, we assume that the magnetic energy density $U_{\rm B} = B_0^2/8\pi$ is in equipartition with the plasma thermal pressure $n_0 k_B T_p$, where $k_{\rm B}$ is Boltzmann's constant; $T_p = T_i + T_e$; and T_i and T_e (~ 50 keV) are the proton and electron temperatures, respectively. T_i is, unfortunately, poorly determined and is chosen to be 10 MeV in this study. The plasma density n_0 is taken to be $\sim 1/(\sigma_T R)$, where σ_T is the Thomson cross section. Since $T_i \gg T_e$, it roughly corresponds to the two-temperature accretion disk situation. However, there have been discussions in the literature questioning whether a two-temperature plasma can occur at all in the accretion plasma (Phinney 1981; Rees et al. 1982; Begelman & Chiueh 1988). We emphasize that we use $T_i = 10$ MeV

only to get a fiducial magnetic field value, and in fact, our model works even better for an isothermal accretion disk because electrons have a much higher thermal speed than protons and are preferentially accelerated (see below).

A tenuous, quasi-spherical extended corona surrounding the hot inner disk is postulated (e.g., Liang & Price 1977; Haardt & Maraschi 1991; Haardt, Maraschi, & Ghisellini 1994). The coronal electron temperature is again taken to be 50 keV initially, and the coronal optical depth $\tau_c = n_c \sigma_T R \lesssim 1$ is varied, where n_c is the coronal electron density. We further assume that the magnetic field in the corona is the same as that in the disk B_0, so that the corona is magnetically dominated and the plasma $\beta \equiv n_c k_B T_p / U_{\rm B}$ is ≤ 1. Notice that $\beta = \tau_c$ with these conditions. Adopting the black hole mass M to be $10 M_\odot$ and the size R of the system to be $\approx 30 GM/c^2$, within which most of high energy emissions are produced, we find that the coronal magnetic field B_0 and dimensionless Alfvén speed $v_{\rm A}/c$ are $\sim 3.7 \times 10^6$ G and $B_0/\sqrt{4\pi n_c m_p c^2} = 0.15 \beta^{-1/2}$, respectively. The $\beta < 1$ condition also implies that the proton thermal speed is always less than $v_{\rm A}$.

Here, we make a key assumption that a fraction of the total available energy goes into generating MHD turbulence. This wave turbulence consists of fast mode and shear Alfvén waves (the slow mode will be heavily Landau damped and will probably not be excited), but it is just the fast mode waves that are relevant for electron acceleration. Fast mode waves propagating obliquely with respect to the ambient magnetic field have a parallel magnetic field component, which can couple strongly (or resonate) with a particle when the parallel phase speed of the wave $\omega/k_\parallel$ is about equal to the parallel component of particle velocity $v_\parallel$; i.e., when $v_\parallel = v_{\rm A}/\eta$, where we have used the dispersion relation for the fast mode waves and η is the cosine of the wave propagation angle. This process is referred to as transit-time damping or magnetic Landau damping (e.g., Stix 1992; Lee & Völk 1975; Achterberg 1981), and a broad-band wave spectrum leads to both rapid wave damping

and particle acceleration (MLM). This process is essentially the resonant form of Fermi acceleration (Fermi 1949). Particle interactions with the parallel magnetic field variations (caused by the waves) can be viewed as either head-on (gaining energy) or trailing (losing energy) "collisions". Head-on collisions occur more often than trailing ones, so that net acceleration results. The resonant condition implies that the acceleration threshold is $v_{\rm A}$. For the coronal plasma, $v_{\rm A}$ is comparable to the electron thermal speed but greater than the proton thermal speed if β is less than 1, so that electrons are preferentially accelerated.

2.2. The Electron and Wave Diffusion Equations and Energy Transfer Rates

To simplify the calculations, we consider an isotropic fully-ionized hydrogen plasma permeated by a homogeneous background magnetic field B_0. At some large scale $\lambda_{\rm inj}$, an unspecified mechanism generates fast mode waves. The evolution of the electron distribution $N(E)$ is given by the Fokker-Planck equation

$$\frac{\partial N}{\partial t} = -\frac{\partial}{\partial E}\left\{\left[\left\langle\frac{dE}{dt}\right\rangle_{\rm acc} + \left(\frac{dE}{dt}\right)_{\rm loss}\right]N\right\} + \frac{1}{2}\frac{\partial^2}{\partial E^2}\left[(D+D_c)N\right] \quad , \tag{1}$$

where E is the kinetic energy. Here, we have neglected the escape and (possible) e^-–e^+ pair production. Those coefficients associated with wave-particle interactions are the systematic mean acceleration rate $\langle dE/dt\rangle_{\rm acc} = p^{-2}\partial[p^2 v D(p)]/\partial p$ and the diffusion coefficient $D = 2v^2 D(p)$, where v and p are the electron speed and momentum, and $D(p)$ is the momentum diffusion coefficient (given below). The other convection term $(dE/dt)_{\rm loss}$ represents the sum of electron energy change rates from inverse Compton scattering and synchrotron (ICS) losses $(dE/dt)_{\rm ics}$ and e-e Coulomb collisions $(dE/dt)_{\rm c}$ (Dermer & Liang 1988), which also give rise to diffusion $D_{\rm c}$ (Spitzer 1962; Dermer & Liang 1988). These are the most important processes for electrons in our parameter regime. The processes that are neglected include: the electron-proton Coulomb interaction since it is much slower than e-e

(when $T_i < 100$ MeV); the diffusion due to Compton scatterings since the electron recoil is typically small and wave-particle diffusion will dominate at high energies; the energy gain due to the convergence of the flow since the accretion time is much longer than dynamic timescale ($\sim R/c$). The momentum diffusion coefficient $D(p)$ for transit-time damping is (MLM)

$$D(p) \;=\; (m_e c)^2 \;\frac{\pi}{16}\;\left(\frac{v_{\rm A}}{c}\right)^2\;c\langle k\rangle\;\zeta\;\left(\frac{p}{m_e c}\right)^2\left(\frac{c}{v}\right)\;F(\mu_0) \tag{2}$$

where m_e is the electron mass, $\zeta = U_{\rm T}/U_{\rm B}$, $U_{\rm T}$ is the fast mode wave energy density, $\langle k\rangle$ is the mean wavenumber of the fast mode waves, $\mu_0 = v_{\rm A}/v$ and $F(\mu_0)$ is basically an efficiency factor, which equals zero when $v \leq v_{\rm A}$ (i.e., when resonance is impossible) and equals $-5/4 - (1+2\mu_0^2)\ln\mu_0 + \mu_0^2 + \frac{1}{4}\mu_0^4$ otherwise.

The evolution of the isotropic wave spectral density $W_{\rm T}$ can be approximated by (see Zhou & Matthaeus 1990)

$$\frac{\partial W_{\rm T}}{\partial t} = \frac{\partial}{\partial k}\left[k^2 D_{\rm W}\frac{\partial}{\partial k}\left(k^{-2}W_{\rm T}\right)\right] - \gamma W_{\rm T} + Q_{\rm W}\delta(k-k_0) \quad , \tag{3}$$

where we have included a term $\gamma(k)$ for the wave damping by the electrons and a term $Q_{\rm W}$ for the injection. The wave damping rate $\gamma(k)$ can be obtained from the relation $\int_0^\infty dk\gamma(k)W_{\rm T}(k) = \int_0^\infty dEN(E)\langle dE/dt\rangle_{\rm acc}$ (cf. equation (2)). Since $\langle dE/dt\rangle_{\rm acc} \propto \langle k\rangle$, this implies that large scale waves (small k) will suffer little loss, and that rapid wave dissipation only occurs when k is sufficiently large.

At steady state, the volumetric wave energy injection rate $Q_{\rm W}$ [ergs cm^{-3} s^{-1}] at $k_0 = 2\pi/\lambda_{\rm inj}$ must equal to the rate at which energy is transferred to smaller scales $\sqrt{2}v_A k_0 \zeta^{3/2} U_{\rm B}$ (MLM). This energy flow is eventually dissipated at higher wavenumbers by electrons, which in turn produce X-ray to gamma-ray emissions. This implies that the volumetric gamma-ray energy production rate $Q_\gamma \sim L_\gamma/(4\pi/3R^3)$, where L_γ is the

gamma-ray luminosity, must be smaller or equal (steady state) to $Q_{\rm W}$. This gives

$$\frac{U_\gamma}{U_{\rm B}} \lesssim 3\ \frac{v_A}{c}\frac{R}{\lambda_{\rm inj}}\ \zeta^{3/2} \quad , \tag{4}$$

where $U_\gamma = L_\gamma/(4\pi R^2 c)$ is the energy density of gamma-ray photons. Letting $\lambda_{\rm inj}/R \sim 0.1$, we obtain $U_\gamma/U_{\rm B} \lesssim 4.5\beta^{-1/2}\zeta^{3/2}$. This implies that in order to get $U_\gamma/U_{\rm B} \sim 0.1$ as suggested by the 60–1000 keV luminosity from Cyg X-1 (Phlips et al. 1996), ζ must be $\approx 0.08\beta^{1/3}$, well within the weak turbulence limit.

Next, we look at the electron energy gain and loss rates. The mean acceleration rate of electrons by the waves is given as (MLM)

$$\langle\frac{d\gamma}{dt}\rangle = \frac{\pi}{4}\ \left(\frac{v_A}{c}\right)^2\ c\langle k\rangle\ \zeta\left(\frac{p}{m_e c}\right)\ G(\mu_0) \tag{5}$$

where $G(\mu_0) = F(\mu_0) + (4\mu_0^2 \ln\mu_0 - \mu_0^4 + 1)/(4\gamma^2)$ when $\mu_0 < 1$ and equals 0 otherwise. The product $\langle k\rangle\zeta$ has to be obtained from the simulations (see next section). The ICS losses can be written as $(d\gamma/dt)_{\rm ics} = -(4/3)(\Theta_p/\tau_{\rm dyn})(1 + U_{\rm ph}/U_{\rm B})(p/m_e c)^2$, where $\tau_{\rm dyn} = R/c$ and $\Theta_p = k_B T_p/m_e c^2$. The soft photon energy density $U_{\rm ph}$ is fixed to be the same as $U_{\rm B}$ in this study. Note that this loss rate may be an overestimate for mildly relativistic particles, thus more careful treatment of the losses will help the acceleration.

When the Coulomb loss timescale is longer than both the acceleration and the ICS cooling timescales, we can define a critical energy γ_c at which acceleration balances radiative cooling, $\langle d\gamma/dt\rangle = |(d\gamma/dt)_{\rm ics}|$, which gives

$$\gamma_c \approx 1.3\times 10^4 (\frac{R}{4.5\times 10^7})\langle k\rangle\zeta \quad , \tag{6}$$

where we have utilized the fact that when $p/(m_e c) \sim \gamma_c \gg 1$, $G(\mu_0)/\tau_c$ is almost constant (ranging from 0.76–1.1) for $0.1 \le \tau_c \le 1$. In order to get substantial acceleration—say $\gamma_c \sim 10$—it must be that $\langle k\rangle\ \zeta$ is $> 8\times 10^{-4}$ (cm^{-1}). This offers a direct test of our simulations.

3. Results

We solve equations (1) and (3) using the Crank-Nicholson method (MLM), and concentrate on the time evolution of particles and waves from the start of wave injection until the steady state is reached, during which waves are constantly injected at $k_0 = 2\pi/(0.1R)$. This period turns out to be always less than or comparable to the dynamic timescale $\tau_{dyn} \sim 1.5 \times 10^{-3}$ sec. This validates our assumption of neglecting escape. The Coulomb loss is fixed at the rate that is corresponding to the initial Maxwellian. Even though this treatment is not self-consistent, our particle acceleration results should not be affected much since Coulomb loss plays a negligible role compared to the ICS cooling at relativistic energies. The Kolmogorov phenomenology for the wave evolution is assumed so that $W_{\rm T} = W_0 k^{-5/3}$ with $W_0 \propto (Q_{\rm W}/v_A)^{2/3} U_{\rm B}^{1/3}$. The injection rate $Q_{\rm W}$ is chosen as $\approx 2.8 \times 10^{15} (v_A/c)$ ergs cm^{-3} s^{-1}, corresponding to $\zeta = 0.2$ *at steady state*, and $U_{\rm T} = \int_0^\infty W_0 k^{-5/3} dk$ should be a constant for all the cases considered here; there are all confirmed by the simulations to within the numerical error.

Figure 1 summarizes the time evolution of the particle density distribution $N(E)$ (upper panels) as a function of kinetic energy E, and the corresponding wave spectral density $W_{\rm T}$ (lower panels) as a function of wavenumber k. Three different densities are considered. Each plot has 16 curves in it, corresponding to 5 evenly-spaced time intervals in each of three periods, $t = 0$–$0.04\tau_{dyn}$, 0.04–$0.16\tau_{dyn}$, and 0.16–$0.6\tau_{dyn}$, respectively. The particle distributions soften first (e.g., curves $1-8$ in $\tau_c = 0.5$ case), due to the fact that acceleration is very inefficient initially since waves have not fully cascaded (i.e., small $\langle k \rangle$ as shown in lower panel), and Coulomb and ICS losses dominate at high energies. As waves cascade over the inertial range, $\langle k \rangle$ quickly grows to a level that acceleration overcomes both Coulomb and ICS losses. Electrons are then energized out of the thermal background and the nonthermal hard tail forms. This is indicated, for example, by curves 6–15 in the

$\tau_c = 0.1$ case. After that, both the particle and wave spectra gradually reach steady states.

The $\tau_c = 0.1$ case clearly illustrates several other points. From simulations, $\langle k \rangle \zeta \sim 10^{-3}$ (cm^{-1}), thus $\gamma_c \sim 10$ using equation (6), which is in perfect agreement with curve 15. Furthermore, the nonthermal tails start to develop only at $E/m_e c^2 \sim 0.13$ (corresponding to $v_\mathrm{A}/c = 0.46$), complying with the acceleration threshold. The threshold energies for $\tau_c = 1$ and 0.5 are buried in the thermal distributions.

That the particle's high energy cutoff gets larger as τ_c decreases can be understood from equation (6). As τ_c decreases, fewer particles are available to absorb the wave energy, which results in larger $\langle k \rangle$. Smaller τ_c also reduces the number of particles with $v > v_\mathrm{A}$, as evident from the upper panels in Figure 1.

Figure 2 shows the fraction of electrons with $E \geq 511$ keV out of the total electron population as a function of coronal optical depth $\tau_c = 0.1$–1, both in energy content $f_{E511} = [\int_{511}^{\infty} EN(E)dE] \,/\, [\int_0^{\infty} EN(E)dE]$ (upper panel), and in number $f_{N511} = [\int_{511}^{\infty} N(E)dE] \,/\, [\int_0^{\infty} N(E)dE]$ (lower panel). The horizontal dashed line indicates the initial values for a 50 keV Maxwellian. Again, we can see that a significant fraction of particles are accelerated into a nonthermal population for $\tau_c \leq 1$.

4. Conclusions and Discussions

We have studied particle acceleration in galactic black hole accretion disk coronae via interactions between electrons and fast mode waves—specifically, via the transit-time damping process. Including Coulomb collisions, inverse Compton scattering and synchrotron losses, we show that particles with speeds higher than the Alfvén speed can be accelerated out of the thermal background, and we obtain steady state particle distributions composed of a Maxwellian plus a nonthermal high energy tail extending into several tens of MeV.

Detailed radiation modeling will be presented in a forthcoming work and we expect that the Maxwellian and the nonthermal tail of the particle distribution will be responsible for the power-law spectra in the tens of keV and the high energy gamma-rays observed from several GBHCs such as Cyg X-1 and GRO J0422, respectively.

The generation of plasma wave turbulence in accretion disk environments is a fairly unexplored topic, but it is reasonable to suppose that the fast mode waves will be excited since it is an intrinsic long-wavelength mode of a magnetized plasma. We emphasize that the coronal plasma β must be < 1 for electrons to get most of the wave energy, otherwise proton acceleration becomes possible, reducing the energy flow to the electrons.

The particle acceleration mechanism discussed here also has direct implications on the high energy radiation from accretion disks in AGNs, notably Seyfert galaxies. Preliminary analyses have indicated that most of our results are insensitive to the size of the system; thus, we expect $>$ MeV emissions are also being produced in Seyferts as well, though high quality spectra above 200 keV are clearly needed to firmly settle this issue.

We thank the referee for many constructive suggestions. Comments from Drs. Edison Liang and Chuck Dermer are appreciated. H.L. gratefully acknowledges the support of the Director's Postdoc Fellowship at LANL. Part of the work was completed during J.A.M.'s visit at LANL, also supported by the same fellowship.

REFERENCES

Achterberg, A. 1981, A&A, 97, 259

Begelman, M.C. & Chiueh, T. 1988, ApJ, 332, 872

Dermer, C. D., & Liang, E. P. 1989, ApJ, 339, 512

Dermer, C.D., Miller, J.A., & Li, H. 1996, ApJ, 456, 106

Fermi, E. 1949, Phys. Rev. 75, 1169

Gary, S.P. 1993, Theory of Space Plasma Microinstabilities (Cambridge: Cambridge University Press)

Haardt, F., & Maraschi, L. 1991, ApJ, 380, L51

Haardt, F., Maraschi, L., & Ghisellini, G. 1994, ApJ, 432, L95

Harmon, B. A. et al. 1994, in The Second Compton Symposium, ed. C. Fichtel, N. Gehrels, & J. Norris (New York: AIP Conf. Proc. No. 304), 210

Lee, M. A., & Völk, H. J., ApJ, 198, 485

Li, H., Kusunose, M., & Liang, E. P. 1996, ApJ, 460, L29

Liang, E. P. 1993, in The first Compton Symposium, ed. M. Friedlander, N. Gehrels & D. Macomb (New York: AIP Conf. Proc. No. 280), 396

Liang, E.P. & Price, R.H. 1977, ApJ, 218, 247

Ling, J. C. et al. 1996, ApJ, *to be submitted*

McConnell, M. et al. 1996, ApJ, *to be submitted*

Miller, J.A., LaRosa, T.N., & Moore, R. L. 1996, ApJ, 461, 445 (MLM)

Phinney, E.S. 1981, in Plasma Astrophysics, ed. T.D. Guyenne & G. Levy (ESA SP-161), 337

Phlips, B. F. et al. 1996, ApJ, 465, 907

Rees, M.J. et al. 1982, Nature, 295, 17

Roberts, D. A., & Wiltberger, M. J. 1995, J. Geophys. Res., 100, 3405

Shakura, N.I. & Sunyaev, R.A. 1973, A&A, 24, 337

Shapiro, S.L., Lightman, A.P., & Eardley, D.N. 1976, ApJ, 204, 187

Skibo, J.G. & Dermer, C.D. 1995, ApJ, 455, L25

Spitzer, L. 1962, Physics of Fully Ionized Gases (New York: Interscience)

Stix, T. H. 1992, Waves in Plasmas (New York: AIP), pp. 273–292

Sunyaev, R., & Titarchuk, L. 1980, A&A, 86, 121

Titarchuk, L. 1994, ApJ, 434, 570

van Dijk, R. et al. 1995, A&A, 296, L33

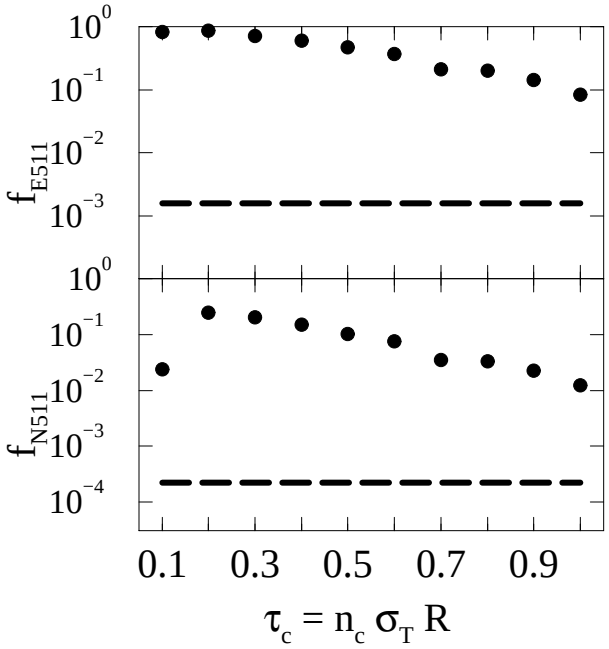
Verma, M. K. 1994, Magnetohydrodynamic Turbulence Models of Solar Wind Evolution, Ph.D. Dissertation, Univ. of Maryland at College Park

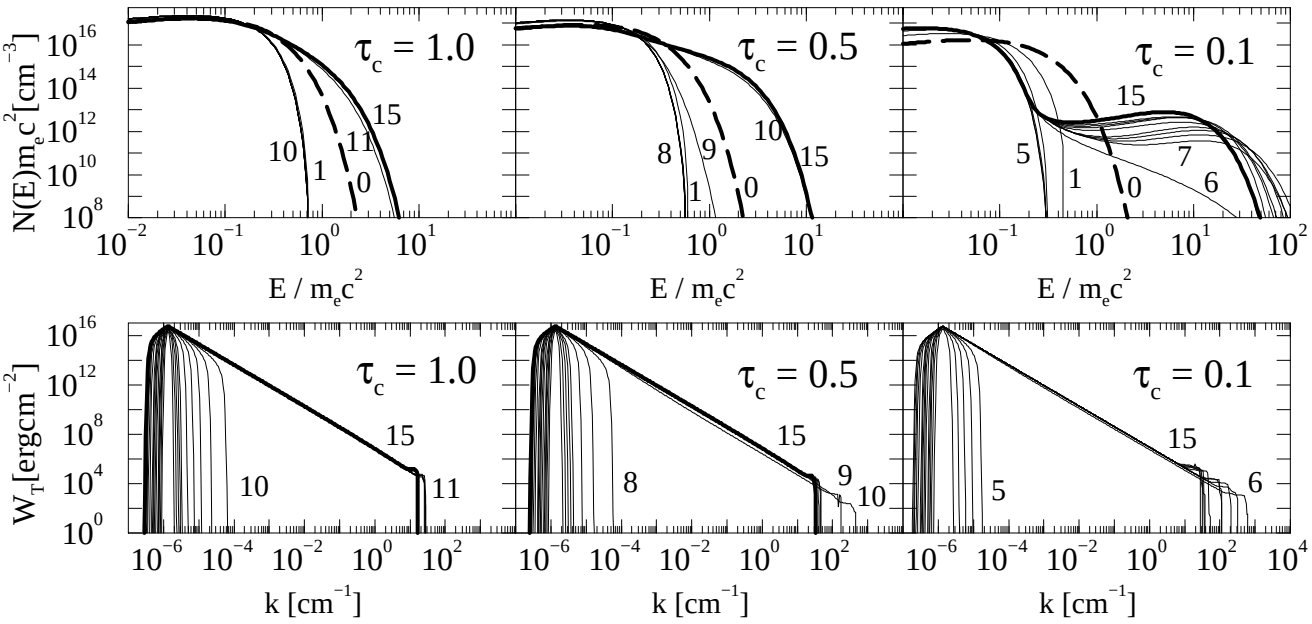
Zhou, Y., & Matthaeus, W. H. 1990, J. Geophys. Res., 95, 14881

This manuscript was prepared with the AAS LaTeX macros v4.0.

Fig. 1.— The time evolution of the electron density distribution as a function of kinetic energy E (upper panels) and wave spectral density as a function of wavenumber k (lower panels). Three coronal plasma densities are considered. There are 16 curves in each plot and the numbers indicate their time-sequence, spanning from $t = 0 - 0.6\tau_{dyn}$, where $\tau_{dyn} \sim 1.5 \times 10^{-3}$ sec. The initial 50 keV Maxwellians are shown as the thick-dashed curves (wave spectrum is zero initially) and the thick-solid curves show the steady state particle and wave distributions. As wave cascade progresses, the mean wavenumber becomes large enough that efficient acceleration results, as indicated by the development of the hard tails beyond the Maxwellian in particle distributions.

Fig. 2.— The fraction of electrons with $E \geq 511$ keV out of the total electron population at steady state for the coronal optical depth τ_c ranging from 0.1 to 1, in both the energy content $f_{\rm E511}$ (upper panel) and the number density $f_{\rm N511}$ (lower panel). The dashed lines indicate the values for a 50 keV Maxwellian. When τ_c is high, electrons are mostly nonrelativistic due to cooling, but a good fraction of electrons becomes relativistic and nonthermal from the wave acceleration when $\tau_c \leq 0.5$.


10^0
10^{-1}
10^{-2}
10^{-3}
f_{E511}
10^0
10^{-1}
10^{-2}
10^{-3}
10^{-4}
f_{N511}
0.1
0.3
0.5
0.7
0.9
$\tau_c = n_c \sigma_T R$


τc = 1.0
τc = 0.5
τc = 0.1
N(E)mec2[cm−3]
E / mec2
WT[ergcm−2]
k [cm−1]